Numerical simulation of a low-enthalpy for mini geothermal power plant operating in Rankine Organic Cycle (ORC) and optimization of system components

Julien Rajomalahy, Lala Andrianaivo, Miadana Vololomihaja Andriamifidisoa and Hasina Ramamonjisoa

Université d'Antananarivo, Ecole Supérieure Polytechnique (ESPA), Petroleum Engineering Department, BP 1500 Antananarivo 101, Madagascar, julienrajomalahy@gmail.com

Abstract

In this study, a friendly computer program was developed to simulate several ORC configurations, using mass, energy and entropy equilibrium. Also, we used the principle of heat transfer and mathematical modeling in turbines, pumps, boilers and condensers for ideal and real situations. The criteria for predicting thermodynamic properties, such as enthalpy and entropy, have been taken from previous work. This friendly software can also be used for teaching applied thermodynamics in undergraduate and other Degree courses. In addition to good accuracy, the developed computer program in this work have several configurations not only Rankine's organic cycles but also other computer programs. Between ideal and real conditions (reversible and irreversible processes) there are more option to choose. All results are obtained by arrogant cycles and operate under reversible conditions such as turbines and pumps with 100% isentropic efficiency. Real conditions (irreversible processes) have been explored for a simulation over time because many computer programs for ORC have been implemented in this option.

Résumé

Dans ce travail, un programme informatique amical a été développé pour simuler plusieurs configurations des ORC, en utilisant les équilibres de la masse, d'énergie et d'entropie. Nous avons utilisé aussi le principe de transfert thermique et la modélisation mathématique dans des turbines, des pompes, des chaudières et des condensateurs pour des situations idéales et réelles. Des critères pour prévoir les propriétés thermodynamiques, telles que l'enthalpie et l'entropie, ont été pris dans des travaux précédents. Ce logiciel amical peut également être employé pour enseigner la thermodynamique appliquée dans des cours d'étudiant préparant la Licence et d'autres diplômes. En plus de la bonne exactitude, le programme informatique développé dans ce travail possède également plusieurs configurations, non seulement des cycles organiques de Rankine mais aussi d'autres programmes informatiques. Entre les conditions idéales et réelles (processus réversibles et irréversibles), il y a encore plus d'options de choix. Tous les résultats sont obtenus par des cycles arrogants et fonctionnent dans les conditions réversibles comme des turbines et pompes avec 100% d'efficacité isentropique. Beaucoup de programmes informatiques pour ORC ont été mis en application dans cette option dont l'exploration des conditions réelles (processus irréversibles) pour une simulation dans le temps.

Keywords: Improvement, ORC, Exchanger, Turbine, Pump, ideal and real cycle, software design, simulation

1. INTRODUCTION

The aim of this work is to find the thermodynamic parameters of the process in a simulation and to create a calculation interface. Many computer programs are available for this purpose, working with different ranges and providing to the user's simple configurations of the ORC. To make ORCs more efficient, many

improvements can be employed, just by altering the basic structure of the thermodynamic cycle to reduce the heat needed or to produce more work. For this purpose, a lateral current collector is used, which fluid exits from the turbine, is used to preheat the fluid, which later goes to the evaporator. These improvements can be used as an isolated or as a whole system depending on the capacity and financial resources of the plant (Çengel, 2013; Potter, 2006).

Figure 1 presents the thermodynamic principle of the Rankine cycle in the form of a *p - h* (pressure - enthalpy) diagram and associated hardware components. The blue curve called the dome of saturation. It delimits the states of the fluid: the fluid is in the liquid, vapor or mixed state depending on whether it is left, right or inside this dome while Speaks of supercritical state when it is above [Chen et al, 2010].
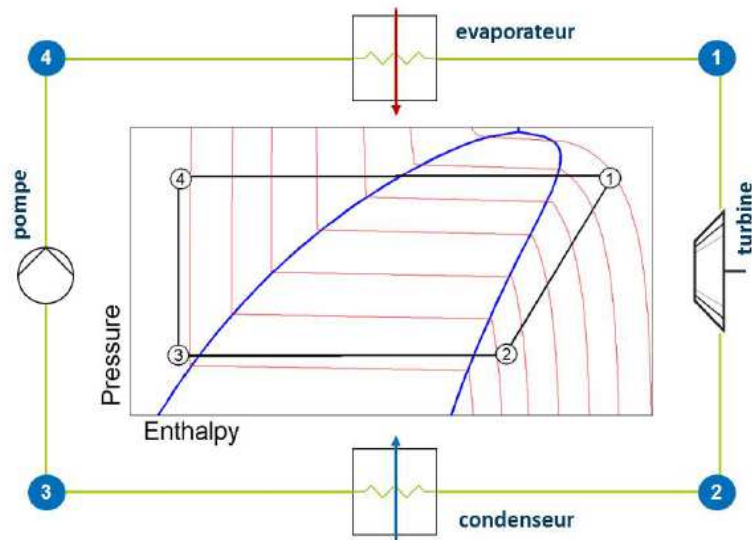

Figure 1: Thermal Principle of the Rankine Cycle (Johan, 2015)

The fluid is pressurized by a pump and then vaporized under the effect of heat through the evaporator. The kinetic energy of the steam under pressure is then recovered by an expansion machine (turbine). The fluid must then be decondensed to return to the pump.

The ORC is distinguished from the theoretical cycle of Carnot by the substitution of the two isothermal transformations by two isobaric transformations which make possible its technical realization. The ideal ORC is thus composed of the following four transformations:

3 - 4: Adiabatic compression (without heat exchange) and reversible (isentropic, i.e. without friction or leakage, etc.).

4 - 1: Isobar spraying (without pressure drop). The evaporator can be divided into three zones: preheating where the fluid is in the liquid state, evaporation (inside the saturation dome) and overheating.

1 - 2: Adiabatic and reversible relaxation.

2 - 3: Isobaric liquefaction.

The characteristics of the fluid used have a major impact on the efficiency of the cycle and the choice of material components [Saleh et al, 2007].

2. WORKING FLUID

In our simulation we used the organic fluid R134a with the following properties (table 1).

In the ORC cycle the fluid changes its state of the liquid to vaporize and vice versa. Therefore, it is necessary to monitor this condition by means of a state equation. Here, in our model we choose the Peng-Robinson

equation of state (equation 8), which identifies the state of the fluid giving a relation of temperature and saturation pressure [Zhao et al, 2011].

Table 1: Property of the action fluid R134a

Name		
ISO Number	R134a	
Chemical Name	1,1,1,2-tetrafluoroethane	
Formula	CF3CH2F	
CAS Number	811-97-2	
Category	halocb	
Molecular Weight	102.032	
Critical Point		
Temperature	101.1	°C
Pressure	4059	kP
Boiling Point		
BP (at 1 atm)	-26.1	°C
Glide (at BP)	0.0	°C
Triple Point		
Temperature	-26.1	°C
Property Range (limits of curve fit)		
Min Temp	-41.5	°C
Max Temp	72.5	°C
Min Pressure	47	kPa
Max Pressure	3526	kPa

3. METHOD OF RESOLUTION

3.1. Ideal thermal cycle

The ideal Organic cycle of Rankine (Figure 2) is a cycle in which the working fluid passes through the components of the cycle without irreversibility. In particular: the pressure drop is absent in the vaporizer, the condenser and the lines. The turbine and the pump are considered isentropic. The processes of the cycle are reversible processes [Zhao et al, 2011].
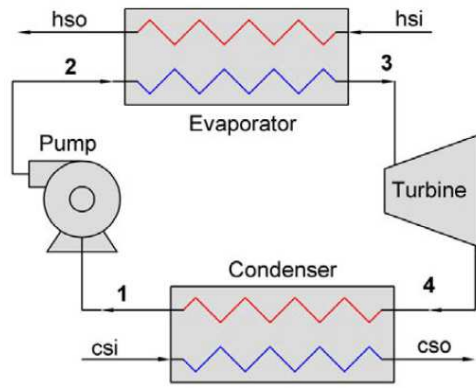
Figure 2: Rankine's ideal organic cycle

The energy balance of the cycle is described by the following equations:

Pump

$$W_p = (h_3 - h_4)\dot{m} \quad (1)$$

Evaporator

$$Q_V = (h_1 - h_4)\dot{m} \quad (2)$$

Turbine

$$W_t = (h_1 - h_2)\dot{m} \quad (3)$$

Condenser

$$W_c = (h_2 - h_3)\dot{m} \quad (4)$$

Network cycle

$$W_{net} = W_t - W_p \quad (5)$$
$$W_{net} = Q_v - Q_c \quad (6)$$

Cycle yeld

$$\eta_{or} = \frac{W_{net}}{Q_v} \quad (7)$$

Equation of state of the action fluid

$$\ln(P_v) = -\frac{a}{T_v} + b \quad (8)$$

The mechanical work performed by the turbine, taking into account the flow rate of the working fluid and the mechanical efficiency of the turbine, is expressed by:

$$W_{mec} = \dot{m}_f W_{net}\eta_{turb} \quad (9)$$

Finally, the electrical power supplied by the alternator, taking into account the mechanical work supplied by the turbine to the alternator and its efficiency is written:

$$W_{elec} = W_{mec}\eta_{alt} \qquad (10)$$

3.2. Thermal cycle with recuperator and flywheel

In the literature, this type of ORC cycle is always simply referred to as the ORC cycle. In this work, we consider two configurations for the subcritical ORC cycle: ORC with a recuperator (Figure 2.a) and with an inertia flywheel (Figure 2.b). The principle of operation of the simple ORC cycle has been explained in paragraph II.1.
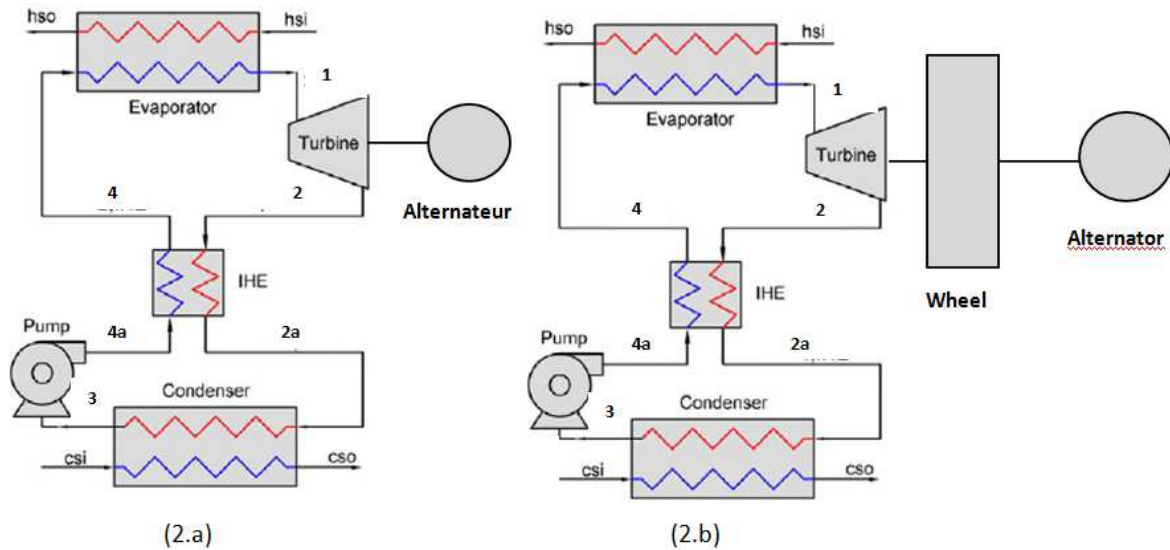

Figure 2: Ideal thermal cycle with recuperator (2.a) and flywheel (2.b)

3.2.1. Modeling the Economizer (recuperator)

In the case where the vapor of the working fluid at the outlet of the turbine is sufficiently hot, an internal heat exchanger (or recuperator) (Figure 3) is added to the bottom cycle. This energy is recovered by exchange with the liquid leaving the pump. This energy recovery thus reduces the quantity of heat required for the preheating of the fluid before it enters the evaporator and the quantity of heat of the working fluid discharged at the cold well and thus the size of the condenser
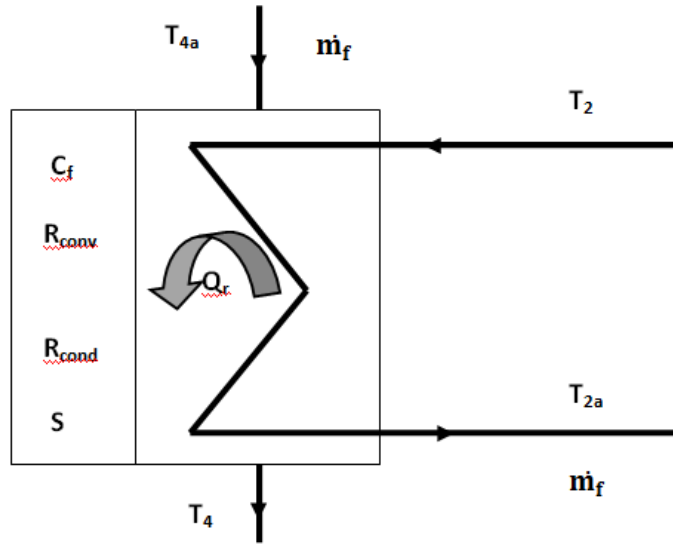
Figure 3: Recuperator Model

Internal functional parameters

$$Q_r : \text{Recuperator heat flow}$$
$$X_r : \text{Proportion of surface of the recuperator}$$
$$P_r : \text{Pressure of the recuperator}$$

Structural parameters

$$S : \text{Surface of exchange}$$
$$R_{cond} : \text{hermal resistance due to metal conduction}$$
$$R_{conv} : \text{Thermal resistance bound to convection}$$
$$C_f : \text{Calorific capacity of the working fluid}$$

By convention, the heat flow is defined as positive

$$Q_r = C_f(T_2 - T_{2a}) \qquad (11)$$
$$Q_r = C_f(T_{4a} - T_4) \qquad (12)$$

The effectiveness of the exchanger is defined by

$$Q_r = \varepsilon C_f(T_2 - T_{4a}) \qquad (13)$$
$$\varepsilon = 1 - e^{-NUT_r} \qquad (14)$$

The number of transfer units involves the overall heat transfer coefficient AU

$$NUT = \frac{AU}{C_f} \qquad (15)$$
$$\frac{1}{AU} = R_{cond} + R_{conv} \qquad (16)$$

3.2.2. Modeling the flywheel

In order to increase the energy obtained in the turbine and also to reduce the mechanical losses. The recovery of the kinetic energy in an inertia flywheel makes it possible to restore the stored energy with more power than before. The rotational speed of the turbine makes it possible to find the geometric factors of the steering wheel [Moyon et al, 2010]. The system requires a clutch method to adapt the speeds involved (Figures 4 and 5).
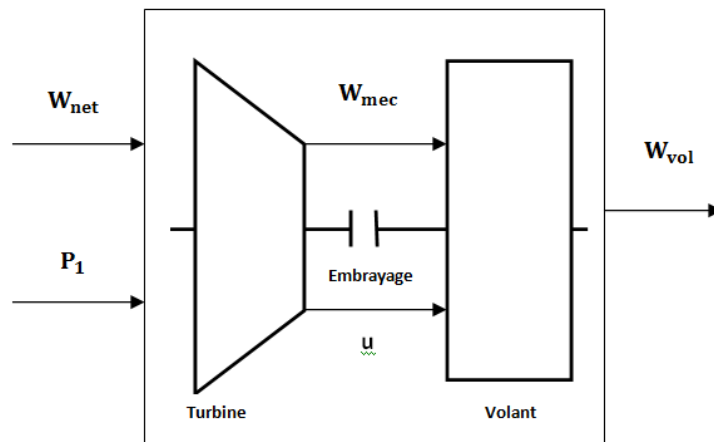
Figure 4: Energy Recovery by Flywheel

Functional parameters

W_{mec} : Work coming out of the turbine

u : Angular rotational speed of the turbine

W_{vol}: Work coming out of the flywheel

Structural parameters
- Turbine

α : Projection angle of C (Absolute speed) to U (speed of drive)

β : Angle between the dissipated energy (W) and the speed of drive (U)

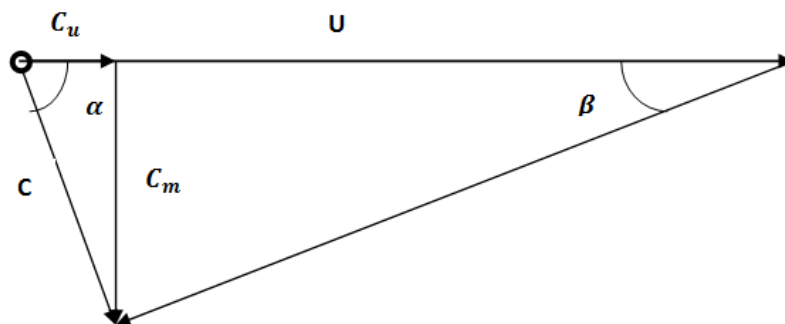D_1 : Diameter of the outer couronne

D_2 : Diameter of the inner courone

Figure 5: Speed Triangle

- flywheel

M : Flywheel mass

d : Energy density

ρ : Volumic mass

r_1 , r_2 : Inside and outside of the flywheel
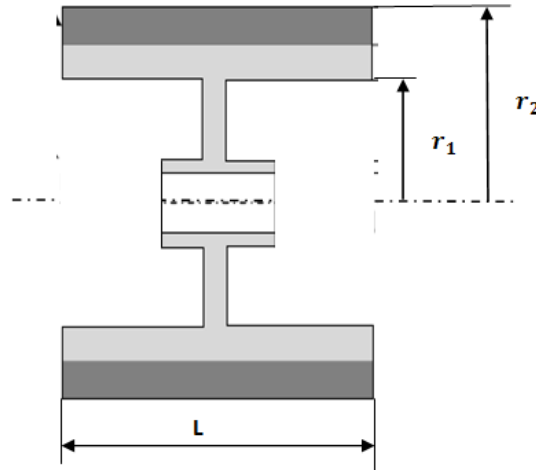
L : Steering wheel width

Figure 6: Dimensions of flywheel

The isentropic efficiency of the turbine is assimilated (possibly to a factor) to the efficiency of the equivalent Laval wheel. The flow rate of fluid is calculated by representing the flow up to the neck of the nozzle. The expansion is then extended to the outlet of the nozzle to define the kinetic energy available at the inlet of the downstream wheel. We thus arrive at the following equations, to which it suffices to add those which define the state variables of the fluid.

$$h_1 - h_2 = \frac{C}{2} \qquad (17)$$

$$C = \frac{\dot{m}V_2}{A} \qquad (18)$$

The performance of the Laval wheel is given by

$$\eta_{turb} = 4\,\frac{U}{C}\,(\cos(\alpha) - \frac{U}{C}) \qquad (19)$$

$$U = \pi D N \qquad (20)$$

The alpha angle and the absolute velocity are defined at the outlet of the nozzle and thus also at the inlet of the Laval wheel.

For the flywheel, the kinetic energy of a material point is given by the following relation

$$dE_c = \frac{1}{2}\omega^2 R^2 dM \qquad (21)$$

With   R : the radius of the trajectory of the point under consideration

        dM :the elementary mass of this point

A flywheel of inertia, or anybody rotating about a fixed axis, has for kinetic energy the sum of the kinetic energies at each point. Since the rotational motion is common to all points, the angular velocity parameter can be set. There then appears the expression of the moment of inertia of the set

$$\iiint dE_c = \iiint \frac{1}{2}\omega^2 R^2 dM \qquad (22)$$

$$\iiint dE_c = \frac{1}{2}\omega^2 \iiint R^2 dM \qquad (23)$$

The kinetic energy of the rotating mass is

$$W_{vol} = \frac{1}{2}I\omega^2 \qquad (24)$$

With ω : Angular velocity (in rad / s)

I : Moment of inertia (in kg.m2) of the mass around the center of rotation

The moment of inertia measures the resistance which opposes a torque tending to rotate the object. (For a cylinder: $I = \frac{1}{2}M(r_1^2 + r_1^2)$ with M the mass r1 the outer radius and r2 the internal radius).

3.3. Real thermal cycle

The actual ORC cycle differs from ideal cycle due to irreversibility in the components of the cycle. Irreversibility and losses are presented with all subsystems of the Rankine Organic Cycle [Schuster et al, 2008].

Systemic analysis is particularly suited to the study of complex systems [Hoareau 2004, Zuel, 2004]. In this case, our system is considered as a complex system in the sense that it is described by many parameters and consists of several interacting subsystems'

Systemic analysis consists of four phases:
Phase 1: Division of the global complex system into elementary (non-complex) subsystems Phase 2: Identification and listing of the functional parameters of the global system and of the subsystems (model inputs and outputs);
Phase 3: Identification and listing of the structural parameters of the subsystems;
Phase 4: Establishment of the set of equations governing each subsystem. They can come from balance sheets, empirical models or correlation functions;
Phase 5: Return to the global system by highlighting a strategy for assembling the equations handling each subsystem.

Once the analysis is complete, we proceed to the modeling of the system as a whole (Figure 7).
Inventory of the functional parameters of the global system: These are the physical quantities allowing the global system to function (Figure 7).

$$T_v : \text{ temperature of the evaporator } (°C)$$

$$T_{sv} : \text{ evaporator output temperature } (°C)$$

θ_{ev}, θ_{sv} : Respectively, the inlet and outlet temperatures of the heat transfer fluid on the evaporator side (°C)
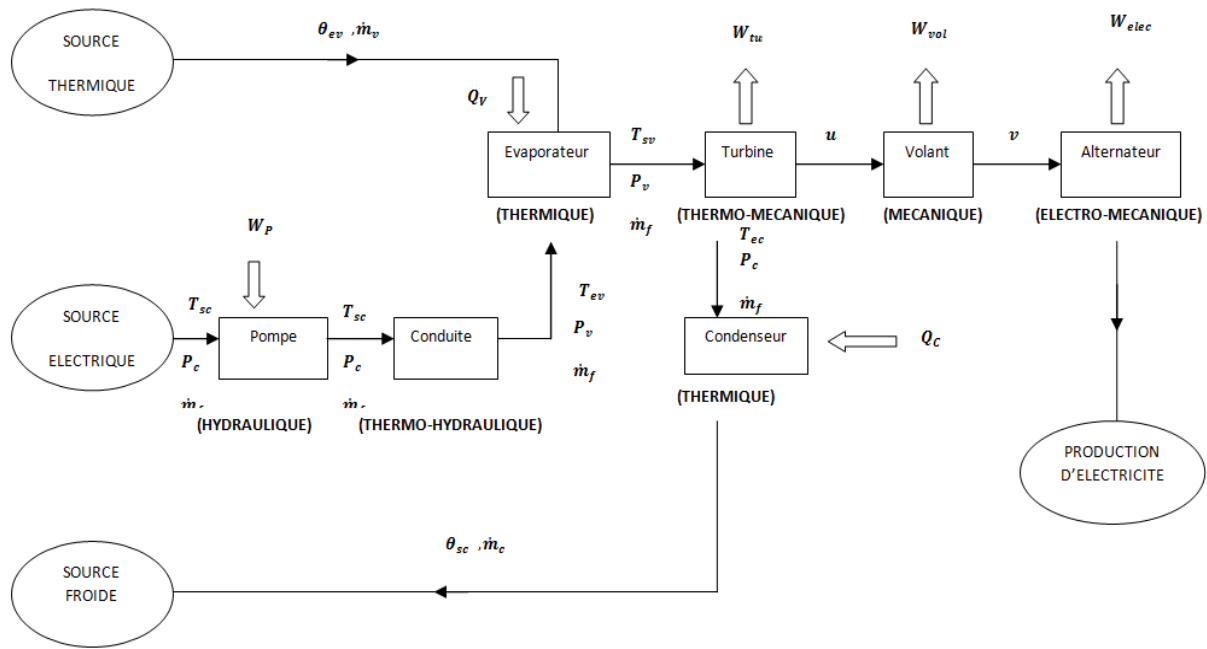
Figure 7: System modeling

$\dot{m}_f$: refrigerant flow rate (kg. s − 1)

P_v : pressure of the refrigerant at the evaporator (Pa)

P_v : pressure at the evaporator (Pa)

W_P : work supplied to the pump (J)

T_c : condenser temperature (° C)

T_{ec} , T_{sc} : temperature of the refrigerant at the inlet and outlet of the condenser (° C)
θ_{ec}, θ_{ev} : respectively, the inlet and outlet temperatures of the heat transfer fluid on the condenser side (°
C)
$\dot{m}_v$: flow rate of the heat transfer fluid at the evaporator (kg. s − 1)
$\dot{m}_c$: flow rate of the heat transfer fluid in the condenser (kg. s − 1)

3.3.1. Modeling of exchangers (Evaporator and Condenser)

In the ideal situation, the sources and sinks of heat are assumed to be, at the level of the evaporator and the
condenser, at temperatures identical to the temperatures of the fluid which passes through the cycle. In the
actual situation, temperature differences must exist in order to allow heat transfers [Tchanche et al, 2009].
These temperature differences are synonymous with creations of entropy and therefore irreversibility.
Fouling increases the temperature gradients required for transfers and thus increases irreversibility.
However, it can be considered that these irreversibility are external irreversibility, linked to sources and
sinks of heat, and consider only the so-called internal irreversibility of the cycle (pump, turbine, friction).

- For the evaporator
In our case, we assume that the evaporator is an exchanger with cylindrical coaxial ducts whose two fluids
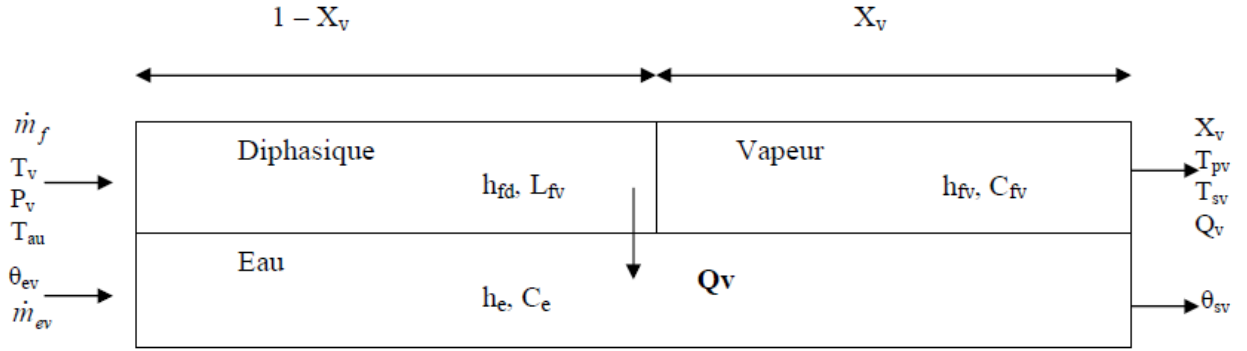circulate in the same direction (Figure 8).

Figure 8: Modeling the evaporator

Internal functional parameters:

Q_v : power exchanged at the evaporator (W),

X_v : proportion of the vapor-to-water exchange surface,

T_{pv} : temperature of the inner wall of the exchanger (° C).

Structural parameters :

S : exchange area (m²)

h_{fd} : convection coefficients of the refrigerant in the diphasic state (W.m².K⁻¹).

h_{fv} : convection coefficients of the refrigerant in the vapor state (W.m⁻².K⁻¹).

C_{fv} : mass calorific capacity of the refrigerant in the vapor state (J.kg⁻¹.K⁻¹)

L_{fv} : latent heat of vaporization of the refrigerant (J.kg⁻¹)

h_e :coefficient of convection of liquid water ((W.m⁻².K⁻¹)

C_e : calorific capacity of liquid water.(J.kg⁻¹.K⁻¹)

The heat exchanged by vaporization and accumulation within the refrigerant fluid is given by the following relation:

$$Q_v \;=\; (1-Tau).\dot{m}_f L_{fv} + C_{fv}.m_f.(T_{sv}-T_v) \qquad (25)$$

The heat exchanged by convection within the refrigerant is given by:

$$Q_v \;=\; h_{fd}.S.(1-X_v).(T_{pv}-T_v) + h_{fv}.S.X_v.(T_{pv} - \frac{T_{sv}+T_v}{2}) \qquad (26)$$

By identification from equations (25) And (26), We have

$$(1-Tau).\dot{m}_f.L_{fv} \;=\; h_{fd}.S.(1-X_v)(T_{pv}-T_v) \qquad (27)$$

$$C_{fv}.mf.(T_{sv}-T_v) \;=\; h_{fd}.S.(1-X_v).(T_{pv}-Tv) \qquad (28)$$

The heat yielded by the heat transfer fluid is given by:

$$Q_v \;=\; \dot{m}_{ev} C_e (\theta_{ev} - \vartheta_{sv}) \qquad (29)$$

The heat yielded by convection by the heat transfer fluid:

$$Q_v = h_e.S.(\frac{\theta_{sv} + \theta_{ev}}{2} - T_{pv})$$
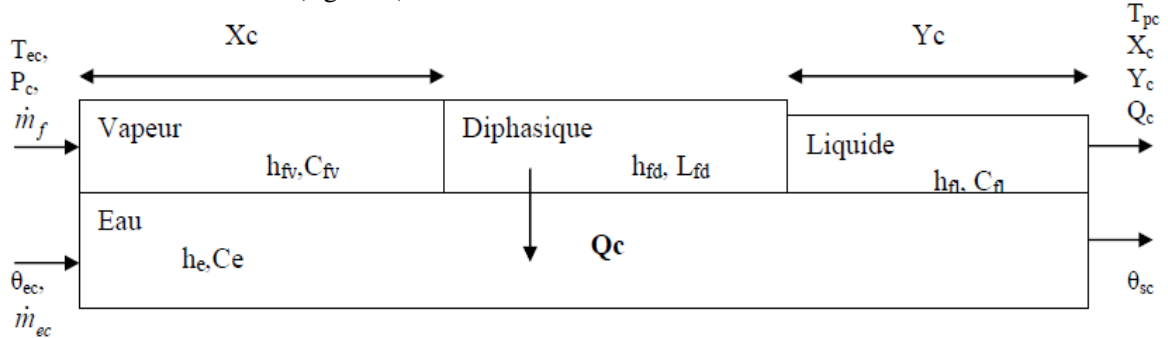
(30)

- For the condenser (figure 9)

Figure 9: Modeling the condenser

Internal functional parameters:

Q_c : power exchanged at the condenser (W)

X_c : proportion of the vapor-to-water exchange surface

Y_c : proportion of the liquid-water exchange surface

T_{pc} : temperature of the internal wall of the exchanger (°C)

Structural parameters:

S : exchange area (m^2)

h_{fd}, h_{fv}, h_{fl} : convection coefficients of the refrigerant in the diphasic, vapor and liquid state respectively (W.m^{-2}.K^{-1})

C_{fv}, C_{fl} : mass calorific capacities of the refrigerant in the vapor and liquid state respectively (J.kg^{-1}.K^{-1})

L_{fd} : latent heat of condensation of the refrigerant (J.kg^{-1})

h_e : coefficient of convection liquid water - wall (W.m^{-2}.K^{-1})

C_e : calorific capacity of liquid water (J.kg^{-1}.K^{-1})

The condenser balance equations:

The heat yielded by condensation of the refrigerant is given by:

$$Q_c = \dot{m}_f.C_{fv}.(T_{ec} - T_c) + \dot{m}_f.L_{fd} + \dot{m}_f.C_{fl}.(T_c - T_{sc})$$

(31)

Balance of convected heat by refrigerant

$$Q_c = h_{fv}.S.X_c(\frac{T_{ec} + T_c}{2} - T_{pc}) + h_{fd}.S.(1 - X_c - Y_c).(T_c - T_{pc}) + h_{fl}.S.Y_c(\frac{T_c + T_{sc}}{2} - T_{pc})$$

(32)

By identification from equations (31) and (32), we have:

$$\dot{m}_f . C_{fv} . (T_{ec} - Tc) = h_{fv} . S . X_c \left(\frac{T_{ec} + T_c}{2} - T_{pc} \right) \qquad (33)$$

$$\dot{m}_f . C_{fl} (T_c - T_{sc}) = h_{fl} . S . Y_c \left(\frac{T_c + T_{sc}}{2} - T_{pc} \right) \qquad (34)$$

The heat exchanged by the heat transfer fluid is given by:

$$Q_c = \dot{m}_{ec} . C_e (\theta_{sc} - \theta_{ec}) \qquad (35)$$

Balance of the heat exchanged by convection by the heat transfer fluid:

$$Q_c = h_e . S . \left(\frac{\theta_{ec} + \theta_{sc}}{2} - T_{pc} \right) \qquad (36)$$

3.3.2. Modeling the turbine

Similar to the pumping process, the irreversibility of the expansion process is also characterized by an isentropic efficiency of the turbine. The heat transfer between the fluid passing through the turbine and the environment is often neglected and the turbine is then considered adiabatic. The work produced by the actual expansion process is smaller than the work in the case of an isentropic process.

After passing through the expander, the working fluid is reduced in pressure and temperature (Figure 10).

$P_c, T_{sc}, \dot{m}_f$ → | **Turbine** | → P_v, T_v

Figure 10: Modeling the turbine

Structural parameters:

R : coefficient depending on the geometric data

$$R = f(\alpha, \beta, D_1, D_2)$$

C_{fl} : calorific capacity of the refrigerant (J.kg^{-1}.K^{-1})

L_{fv} : latent heat of vaporization of the fluid(J.kg^{-1})

Equation of behavior (isenthalpic relaxation):

$$P_v - P_c \ = \ \dot{m}_f^{\,2} . R \qquad (38)$$

$$Tau \ = \ C_{fl} . \frac{T_{sc} - T_v}{L_{fv}} \qquad (39)$$

3.3.3. Modeling the pump

Pumping is accompanied by an increase in entropy. The work required by the actual process is therefore more important than in the case of the ideal process. The heat transfer between the fluid passing through the pump and the environment is often neglected and the pump is then considered adiabatic. The irreversibility in the pump is therefore characterized by the isentropic efficiency.

Due to compression, the temperature and pressure of the refrigerant increase (Figure 11):
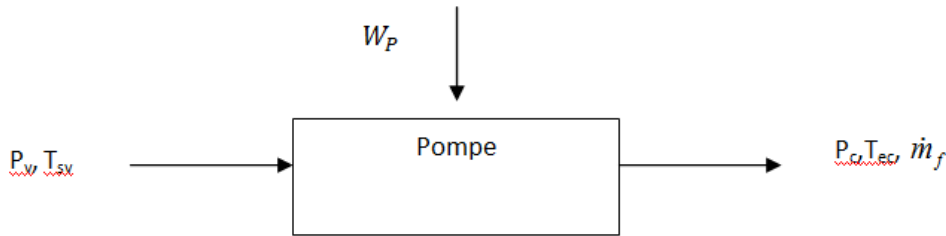

Figure 11: Modeling the pump

Structural parameters:

γ : isentropic pumping coefficient specific to the fluid

$$\gamma = \frac{C_p}{C_v} \qquad (40)$$

Knowing that the pumping is isentropic, we have:

$$T_{ec} = T_{sc}(\frac{p_c}{p_v})^{\frac{\gamma-1}{\gamma}} \qquad (41)$$

3.3.4. Modeling of the friction of the working fluid

Internal friction and friction with the walls inherent in the flow of the working fluid cause pressure drops in the evaporator, the condenser and the connecting pipes between the components of the cycle. To compensate for these pressure drops, the working fluid must be pumped at a higher pressure than the pressure demanded by the ideal cycle. This increases the size of the pump and therefore its power.

In Bernoulli's theorem, if the flow goes from 1 to 2 [Zotto, et al., 1996]

$$W_{1\rightarrow2} + X_1 = X_2 + Z_{1\rightarrow2} \qquad (42)$$

With the hydraulic load defined by (with i the point considered in the circuit):

$$X_i = P_i + \frac{1}{2}\rho v_i^2 + \rho g z_i \qquad (43)$$

The total pressure drop is defined by

$$Z_{1\rightarrow2} = J_{1\rightarrow2} + Y_{1\rightarrow2} \qquad (44)$$

With linear head losses

$$J_{1\rightarrow2} = \lambda\rho v^2 \frac{1}{2}\frac{L}{D} \qquad (45)$$

And singular pressure drops

$$Y_{1\rightarrow2} = \sum_{i=1}^{n} \xi_i \rho \frac{v^2}{2} \qquad (46)$$

We can thus define the pressure drops at each point of the network and thus deduce the electric power consumed by the pump, depending on the work to be provided to combat the head losses.

3.4. Resolution and simulation parameters

We are dealing with a system of non-linear equations of 22 unknowns for 22 equations. These unknowns are:

Qv, Tau, f $m\&$,Tsv, Tv, Tpv, θsv, Pv, Xv,

Qc, Pc, Tec, Tc, Tsc, Tpc, θsc, ,Xc,Yc

One of the possible ways to solve and solve this system block is the use of a solver. But given the very large interaction that binds the factors, only data corresponding to real experimental conditions make it possible to initialize the system and then to approach an operating point and converge the system over time. Considering the systemic approach of this study, we can detail the system to establish a relation between each unknown and each equation. This technique allows to linearize as much as possible the methods of resolution.

The model is solved under the MATLAB environment, taking into account the different equations developed in steady-state and dynamic conditions, in order to have the most comprehensive approach possible. The software also allows to have a graphical interface (Figure 14) which allows the visualization of the various variables as well as the evolution of the performance of the process. The calculations are carried out and then posted on the interface. Table 2 gives the list of simulation parameters.

Table 2: lists of simulation parameters

Fonctional parameters	Evaporator	- Inlet temperature T_v(°C): 60
	Pump	- Pressure of entry P_c (Bar): 7.7
		- Pressure of exit P_v (Bar): 18
	Condenser	- Inlet temperature T_c(°C): 30
	Geothermal sources	- Heat θ_{ev}(°C): 90
		- Cold θ_{ec} (°C):15
Structural parameters	Evaporator	- Heat-transferring surface S (m^2): 69.01.10^{-2}
		- Types: Cylindrical exchanger coaxial (fluid of the same direction)
		- Convection coefficients (Wm^{-2}K^{-1}) : h_e =90.64 / h_{fv}=142.51 /h_{fl}=150.55
		- Mass heat-storage capacity R134a (JKg^{-1}K^{-1}) : $C_{pliquide}$ = 1382 / $C_{p\ gaz}$ = 848.2
		- Latent heat of vaporization (J.kg^{-1}) : L_{fd} = 192 266
	Turbine	- Jetting angles :$\alpha = 19°08 \beta = 39°01$
		- Crown external and interior (mm): D_2=150 et D_1=50
		- Output $\eta_{turb} = 0,95$
	Condenser	- Heat-transferring surface (m^2) : S=69.01 10^{-2}
		- Types: Cylindrical exchanger coaxial (fluid of the same direction)
	Pump	- Isentropic coefficient of pumping $\gamma = 1.169$
		- Output $\eta_{pompe} = 0,9$
	Wheel	- Mass (Kg) M=50

		- Density of energy (Wh/Kg) **d**=6 - Density (Kgm^{-3}) $\rho_{volant} = 2240$ - Interior and external ray (mm) **r₁**=200 et **r₂**=100 - Width (mm) **L**=150
	Alternator	- Output $\eta_{alt} = 0,80$
	Conduits	- Diameter (mm) **D**=20 - Absolute roughness (mm) $\varepsilon = 0.05$ - Density of the water and the working liquid (Kgm^{-3}) - Speed of the water and the working liquid (ms^{-1}) - Viscosity of the water and the working liquid
Flows parameters	Flow of the working liquid (Kgm^{-1})	m_{fc}=0.045 m_{fv}=0.045
	Flow of the thermal source (Kgm^{-1})	$m_{eau\ géothermiques}$=0.0133
	Flow of the cold source (Kgm^{-1})	$m_{source\ froide}$=0.0166

4. RESULTS AND INTERPRETATIONS

4.1. Comparison Chart on Energy Efficiency

Table 3 shows the Comparison of cycles.

Table 3: Comparison of cycles

Type of cycle	Temperature [°C]						Titrate	Useful electrical energy [KW]
	1	2	2a	3	4a	4		
Simple cycle	65	30	-	28	-	30.41	0.99	295.16
Cycle with recuperator	73	30.1	30	29	40	30.50	1	318.11
Cycle with wheel of inertia	65	30	-	29	-	30.50	0.99	348.92
Cycle with recuperator and wheel of inertia	73.01	29	28.9	28.8	40.01	30.41	1	357.21

There is an increase in useful energy after addition of economizer and flywheel (Table 3) from 7.8% to 21%. The simulation gives the value of the temperatures at the output of the components, the most important and that of the exchanger which varies from 65 to 73 ° C. The flywheel affects only the useful energy (There is accumulation and conservation of energy 295.16 KW at 348.92 KW).

Table 4 shows that the result converges starting from the actual initial data introduced. In this simulation case, the value of T_{sv} and T_{sc} is recalculated from equations 28 and 32. The system is stable over time and obtains the approach of an operating point.

Table 4: Simulation of the real cycle over time

	t=1	t=2	t=3	t=4	t=5	t=6	t=7	t=8	t=9	t=10	…..
Q_v	724.1404	721.5989	723.9046	721.8073	723.7216	721.9848	723.5694	722.1313	723.4427	722.2521	….
$θ_{sv}$	50.9900	50.0357	50.9943	50.0320	50.9976	50.0288	50.0003	50.0261	50.0026	50.0240	….
T_{pv}	65.9180	65.9815	65.9239	65.9763	65.9285	65.9719	65.9323	65.9682	65.9355	65.9652	….
X_v	0.0671	0.0830	0.0693	0.0819	0.0704	0.0808	0.0713	0.0800	0.0721	0.0792	….
T_{sv}	65.6107	66.1016	66.6804	65.0692	67.7172	65.0385	65.7470	65.0128	66.7715	65.9914	….
T_{ev}	30.2741	30.8750	30.3594	30.8353	30.4045	30.7977	30.4409	30.7663	30.4709	30.7402	….
Q_c	1067.99	1069.26	1067.69	1069.05	1067.81	1068.94	1067.91	1068.85	1068.0	1068.78	….
$θ_{sc}$	25.3733	25.3915	25.3690	25.3885	25.3706	25.3869	25.3722	25.3856	25.3734	25.3845	….
T_{pc}	15.6124	15.6012	15.6150	15.6031	15.6140	15.6040	15.6130	15.6048	15.6123	15.6055	….
X_c	0.0217	0.0221	0.0217	0.0220	0.0217	0.0220	0.0218	0.0220	0.0218	0.0220	⋯
Y_c	0.0469	0.0462	0.0465	0.0462	0.0464	0.0462	0.0464	0.0462	0.0464	0.0462	⋯
T_{sc}	29.1666	29.0999	29.1761	29.1093	29.1704	29.1666	29.1653	29.1192	29.1610	29.1229	….
T_{au}	0.1887	0.1883	0.1888	0.1883	0.1888	0.1884	0.1887	0.1884	0.1887	0.1884	⋯

4.2. Representation on the Mollier Diagram

The Figure 12 gives the enthalpy diagram of the simple cycle without economizer. For step (4-1) the vaporization stops for the enthalpy of 440 KJ / Kg. The cycle then performs isentropic expansion up to 410 KJ / Kg.
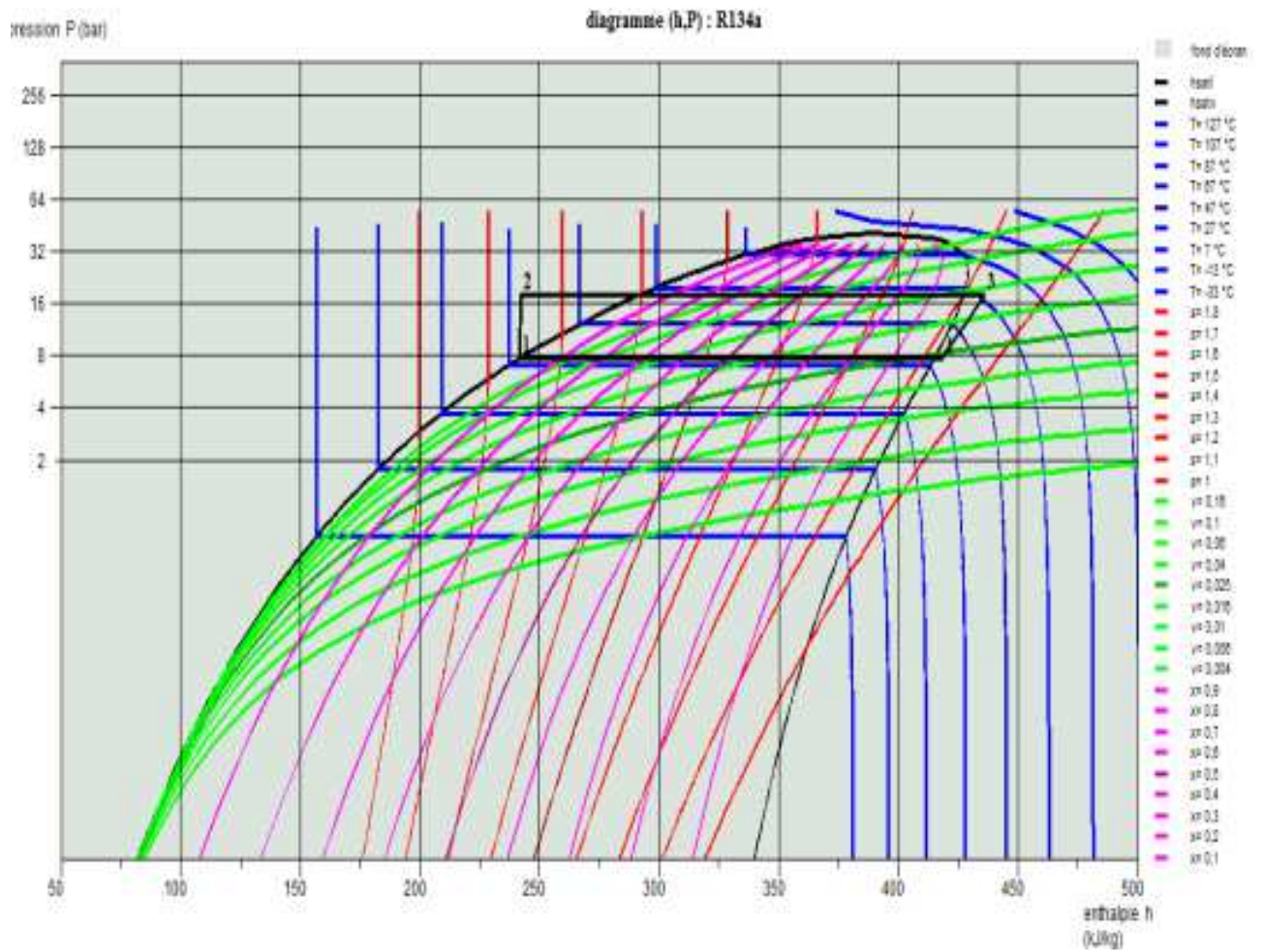
Figure 12: Enthalpy diagram (P H) of the ideal simple cycle

In Figure 13, an enthalpy diagram of the cycle with economizer is also obtained. Afterwards, the course (4-1) stops for the enthalpy of 470 KJ / Kg. Then the trigger stops at 430KJ / Kg.
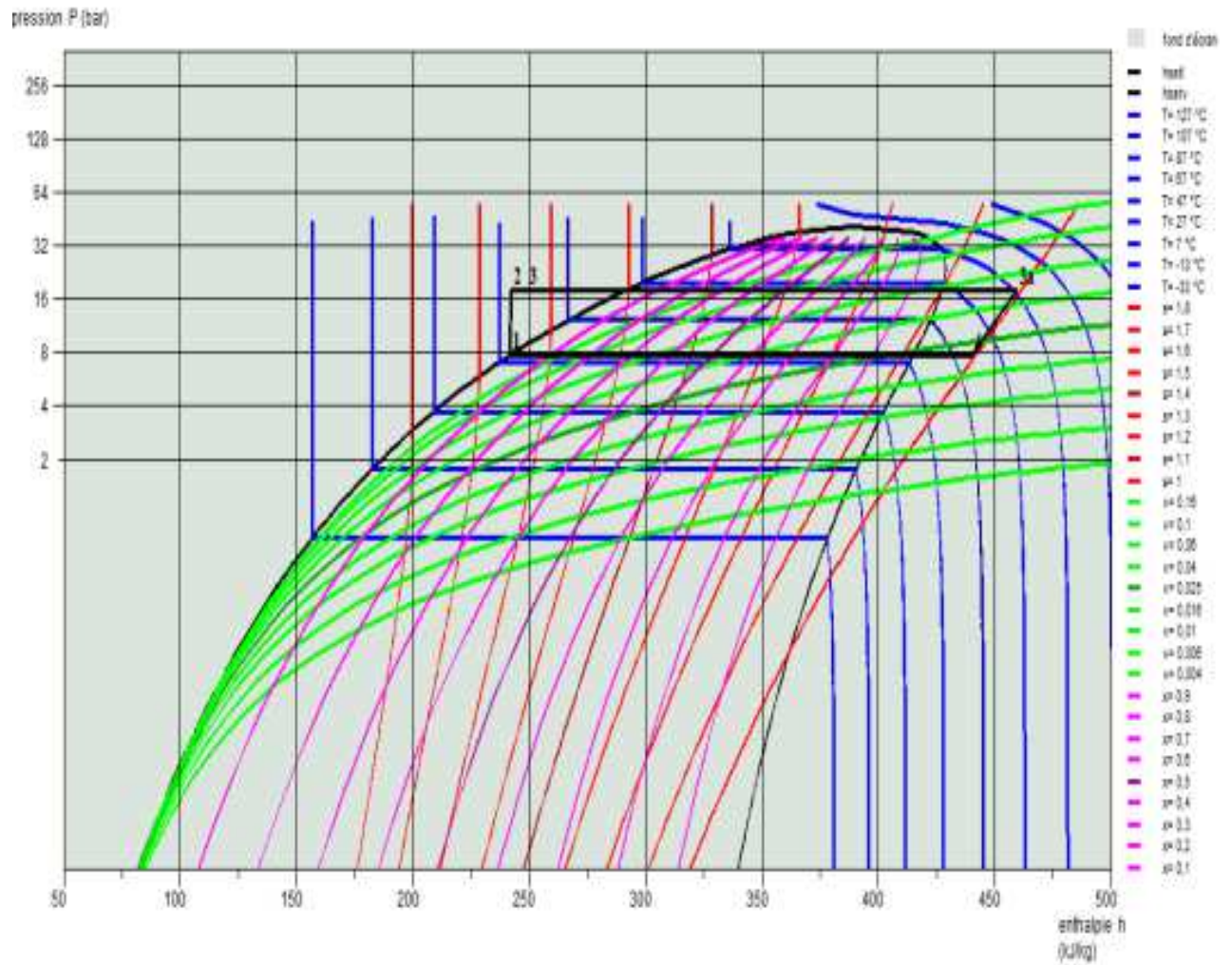
Figure 13: Enthalpic diagram (P H) of the cycle with ideal economizer

4.3. Graphical simulation interface

Figure 14 shows the representation interface after thermodynamic simulation.
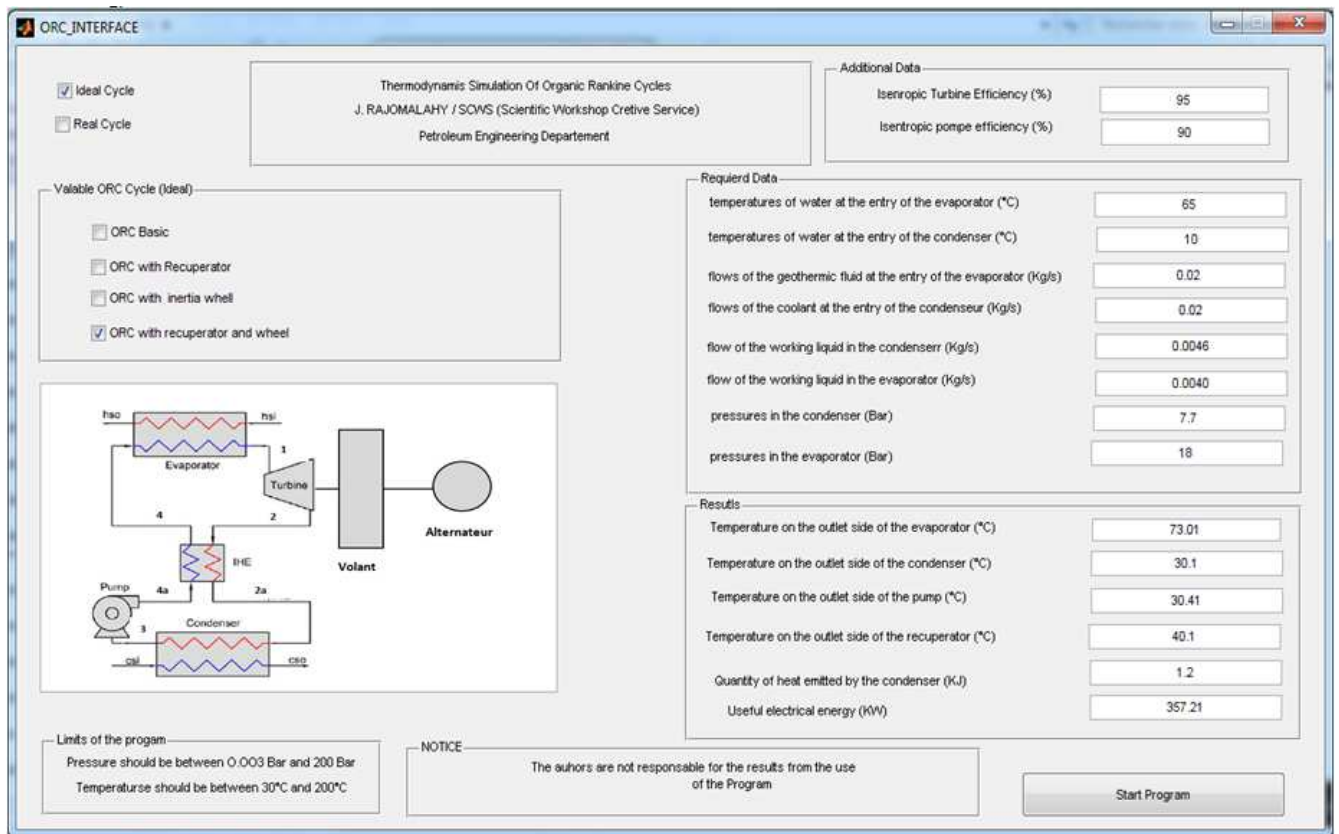
Figure 14: Representation interface after thermodynamic simulation

5. DISCUSSION

Based on the previous tables it is possible to observe that the computer program developed in this work provides results more accuracy and very similar to the results of the other computer [http://www.engr.siu.edu / Staff1 / weston / thermo / Rankine / RankineCycles.html; Accessed in May 27, 2015] and to the examples of books [Milton, 1986]. The relative errors between the sources are smaller than 2.0% in all the ORC configurations obtained by the thermodynamic simulation in this work.

By analyzing the results and input values of pressure and temperature, it is observed that at moderate pressure and temperature values, such as bar 30 and 65ºC, the error between the sources is small and less than 1.0%. The higher the pressure and temperature values, the more they come to the critical point of the working fluid (101.1ºC and 4050 KPa), relative errors increase. This is due to differences in the reference states used to analyze the thermodynamic properties of the fluid in this work and other research. In previous work for the prediction of thermodynamic properties, the authors obtained different values of the thermodynamic properties of the fluid at different reference states. Thus, each computer program uses different tables of thermodynamic properties to simulate its steam power cycles. At low pressure values, the difference is minimal. However, at high pressure values, the difference between the values of thermodynamic properties, such as enthalpy and entropy, increases, causing relative errors more considerably than 1.0%.

Additionally, errors can also occur due to the interpolation method used in the program code in MatLab to predict the thermodynamic properties of the working fluid. However, when this source of error is so great the results continue to be accurate.

6. CONCLUSION

In this study, we simulate the behavior equations of the ORCs for the production of electricity, in order to create a manipulation interface and define an operating point. Scientific knowledge of several potential ORC configurations was addressed with a technical configuration of the different configurations. The other provisions of the CROs also provide interests for the transformation of heat into electricity but still requires efforts for the feasibility and profitability of the system.

REFERENCE

Journal papers

Arce P, Freire N., 2016: Programming and testing of a friendly GUI-MatLab software to predict the thermodynamic properties of water, *International J. of Research in Engineering and Technology,* 5 (11), 52-57

Schuster A., Karellas S., Aumann R., 2010: Efficiency optimization potential in supercritical organic Rankine cycles, *Energy,* 35, 1033-1039.

Chen H, Goswami D.T., Stefanakos E.K., 2010. A review of thermodynamic cycles and working fluids for the conversion of low-grade heat. *Renew Sustain Energy*, 14, 3059–3067

Saleh B., Koglbauer G., Wendland M, Fischer J., 2007. Working fluids for low-temperature organic rankine cycles. *Energy*, 32 (7), 1210 – 1221

Zhao X., Wang C., Li Y., 2011. Modeling and model order reduction of evaporator in organic rankine cycle for waste heat recovery. In *IEEE Advanced Mechatronic Systems (ICAMechS)*, 291–296.

Schuster S.,2008. Supercritical fluid parameters in organic Rankine cycle applications, *International Journal of Thermodynamics,* 11, 101-108

Tchanche B. F, Papadakis G., Lambrinos G., and Frangoudakis A., 2009: Fluid selection for a low-temperature solar organic Rankine cycle, *Applied Thermal Engineering,* 29, 2468-2476

Conference, Letter, Newspaper

Energy Information Administration U.S. Dept. of energy, 2012 : *Annual Energy Outlook* 2, June 2012, DOE/EIA-0383

Hoareau Y, 2003-2004 : Projet énergétique : La pompe à chaleur, *Université de La Réunion*, MPPA.

Zuël O., 2003–2004 ; Projet de modélisation d'une pompe à chaleur sous simulink, *Université de La Ré*union, MPPA

Zotto P. D., Larre J., Merlet A., and Picau L., 1996: Memotech, Genie Energetique, Casteilla,

Milton G.H., 1986: Problemas Resueltos Examenes - *UNI y Otros* (Lima, Perú: EdicionesHabich,).

Reports

Çengel, Y.A., Boles, M.A., 2013: *Termodinâmica* .Porto Alegre, Brazil : McGraw Hill Publishers

Potter, M.C., Scott, E.P., 2006: *Termodinâmica*. São Paulo, Brazil : Thomson Learning

Annual US. & global geothermal power production report, Washington (DC, USA), 2015: Geothermal Energy Assoc.; 2015

Moyon S., Monlaurd F. et Leon M., 2010 : Etude de la récupération de l'énergie cinétique d'un véhicule. Institut National Des Sciences Appliquées De Rouen, Département Sciences et Techniques Pour l'Ingénieur

Webography

http://www.engr.siu.edu/staff1/weston/thermo/Rankine/ RankineCycles.html; accessed in May 27, 2015.